



Article

# Chemical Reduction of GO: Comparing Hydroiodic Acid and Sodium Borohydride Chemical Approaches by X-ray Photoelectron Spectroscopy

Wei Liu<sup>1</sup> and Giorgio Speranza<sup>2,3,4,\*</sup>

<sup>1</sup> MERLin, School of Chemistry, Edgeworth David Building, Level 2, The University of Sydney, Sydney, NSW 2006, Australia; w.liu@unsw.edu.au

<sup>2</sup> Fondazione Bruno Kessler, Sommarive Str. 18, 38123 Trento, Italy

<sup>3</sup> Department of Industrial Engineering, University of Trento, Sommarive Str. 9, 38123 Trento, Italy

<sup>4</sup> IFN—CNR, CSMFO Lab., Alla Cascata Str. 56/C Povo, 38123 Trento, Italy

\* Correspondence: speranza@fbk.eu

**Abstract:** The efficiency of two wet chemical processes based on hydroiodic acid (HI) and sodium borohydride (NaBH<sub>4</sub>) used to reduce graphene oxide (GO) have been studied. At this aim, the oxygen abundance of reduced graphene oxide (rGO) was studied as a function of the reductant concentration. A number of rGO samples were produced and their chemical compositions were studied using X-ray photoelectron spectroscopy. The analyses show that the reduction of the oxygen concentration proceeds non-linearly. At the beginning, when pristine GO is utilized a higher extent of reduction is obtained. The oxygen concentration decreases from ~32% to 10.5% by increasing the HI concentration to 0.24 M. A steeper reduction was observed for NaBH<sub>4</sub>, where the oxygen concentration lowers to ~13.6% using just 50 mg of NaBH<sub>4</sub>. Next, reduction reactions performed with increasing amounts of reductants in aqueous suspensions show a progressive saturation effect, indicating a limit in the final oxygen concentration. We obtained a residual oxygen concentration of 5.3% using 7.58 M of HI and 8.6% with 1200 mg of NaBH<sub>4</sub>. The chemical analysis highlights that the reduction of the oxygen concentration in rGO samples is mainly derived from the cleavage of C-OH bonds and the next reconstruction of C-C bonds.

**Keywords:** reduced graphene oxide; hydroiodic acid; sodium borohydride; XPS; chemical analysis



**Citation:** Liu, W.; Speranza, G. Chemical Reduction of GO: Comparing Hydroiodic Acid and Sodium Borohydride Chemical Approaches by X-ray Photoelectron Spectroscopy. *C* **2022**, *8*, 20. <https://doi.org/10.3390/c8020020>

Academic Editors: Carlo Mariani and Gil Goncalves

Received: 10 February 2022

Accepted: 18 March 2022

Published: 22 March 2022

**Publisher's Note:** MDPI stays neutral with regard to jurisdictional claims in published maps and institutional affiliations.



**Copyright:** © 2022 by the authors. Licensee MDPI, Basel, Switzerland. This article is an open access article distributed under the terms and conditions of the Creative Commons Attribution (CC BY) license (<https://creativecommons.org/licenses/by/4.0/>).

## 1. Introduction

Graphene is a material that has raised the attention of the scientific community for its exceptional properties such as its outstanding electron conductivity, excellent mechanical strength, superior thermal conductivity, and high surface area [1,2]. More than two decades of research on graphene led to a number of patents regarding both its application and production methods. However, the use of graphene on a large scale is strictly dependent on the possibility of producing sufficient amounts of material to satisfy the industrial needs.

At present, the production of graphene flakes has reached thousands of tones/year and the fabrication of continuous graphene sheets with dimension of meters are available [3], allowing for its exploitation in various industrial applications. The rich list of chemical reactions utilized to functionalize the GO sheets enables a large variety of uses in different areas [4,5]. The covalent functionalization of GO sheets includes the transformation of hydroxyl-based functional groups to increase the density of more reactive carboxyl groups, or to produce esters, involving reactions with amide or isocyanate. This permits the further functional modification of the GO surface chemistry using organic molecules [6]. The non-covalent functionalization of GO offers a rich selection of functional groups that can interact via hydrogen, electrostatic, and  $\pi$ - $\pi$  interactions with the GO basal plane. This opens up the possibility to attach complex molecules such as proteins, DNA, drugs, and

amine-terminated polymers. GO may also be considered as a precursor for the fabrication of complex systems by adding nanoparticles, organic compounds, or biomolecules. Metallic nanoparticles, such as Au, Pt, Ru, TiO<sub>2</sub>, and ZnO, etc., are added to improve the catalytic and electrochemical properties of GO [4]. Organic molecules, such as porphyrins, aromatic dyes, alkylamines, ionic liquids, pyrene, perylenediimide, and cyclodextrins, etc., are added to improve the solubility of inorganic solvents, processability in composites, and photoactive or electroactive properties [7]. Biomolecules are added to improve biocompatibility, to fabricate bioelectrodes and biosensors, and for general bioapplications [4,8,9]. Another important application of GO is the fabrication of composites to enhance the mechanical, electrical, and electrochemical properties of materials [10,11]. GO is also utilized in protective coatings against high energy radiation and corrosion [12,13]. Environment and energy are hot research areas due to the present emergency caused by climate change. GO is utilized for environmental remediation by absorbing toxic substances [14–16]. As for energy applications, GO and graphene are emerging as important components [17–19]. In this respect, the doping of graphene, for example, with N atoms [20] is used to modify its electric properties, thus allowing a higher efficiency in energy storage devices such as supercapacitors, batteries, and fuel cells [21].

A significant quantity of graphene particulates is produced using chemical exfoliation processes. However, the exfoliation routes have, as a side effect, the production of highly oxidized, micro/nano sized sheets. The high degree of surface oxidation ensures an easy dispersivity in water, but the high degree of oxidation is also linked to a loss of the original graphene properties. GO sheets are transparent, mirroring the presence of a bandgap whose amplitude varies from 0.02 to 2 eV, depending on the oxygen concentration [22,23] and on the kind of carbon–oxygen bonds [24]. Crystalline graphene, is formed by the dense packing of carbon atoms into a honeycomb lattice. In this lattice structure, the carbon configuration is described by the sp<sup>2</sup> hybridization. The reaction with oxygen atoms leads to a change of the hybridization from sp<sup>2</sup> to sp<sup>3</sup>. Electrons involved in the C–O bonds lose their mobility and the C–O bond becomes a scattering site. This is mirrored by a reduction of the carrier mobility from 10<sup>5</sup> cm<sup>2</sup>/Vs of a single, pure graphene sheet [25] down to 0.05–200 cm<sup>2</sup>/Vs in graphene oxides [26]. In addition, the mechanical properties are affected by the presence of surface oxidation. Pristine graphene sheets possess a Young modulus as high as 1 TPa [27], which decreases to 380–470 GPa in the case of GO sheets [28].

The promise of recovering the original graphene properties by reducing graphene oxide led to intense research. The reduction of GO results in two main effects that are strictly related each other: the loss of material transparency and the recovery of a certain degree of conductivity. The increasing extinction coefficient with the removal of oxygen atoms reflects the recovery of the graphene structure. The peculiar electronic configuration described by the Dirac cones at the K and K' points of the hexagonal Brillouin zone results in a high light absorption. Despite graphene is just one atom thick, it absorbs a significant fraction of incident white light ( $\pi\alpha = 2.3\%$ ) [29]. In rGO, the density of the functional groups is found to deeply affect the absorption coefficient [30]. The decrease of the bandgap with the extent of reduction may change from 1.69 eV to a fraction of eV [31,32]. As a consequence, if functional groups are retained on the surface, rGO becomes a semiconductor thanks to the regeneration of the planar structure [33]. As seen above, the carrier mobility in the presence of oxygen functional groups may be of the order of 100–200 cm<sup>2</sup>/Vs due to electron delocalization [34,35]. This electron mobility is two orders of magnitude bigger than that of organic semiconductors, which typically is less than 1 cm<sup>2</sup>/Vs, preventing their utilization despite the low cost and flexibility. With the recovery of the carrier mobility in rGO, a correspondent increase in the material conductivity is obtained [36], thus making rGO interesting for applications in electronics and conductive composites [37].

Therefore, an efficient elimination of oxygen species from GO is important for any application involving the electronic properties of rGO [11,37,38]. Aiming at obtaining an efficient reduction, a variety of reducing agents have been explored [39]. rGO was synthesized using hydrazine [40], ascorbic acid [41], H<sub>2</sub>S [42], NaBH<sub>4</sub> [43], hydrohalic acid [44],

metal iodide [45], and amino acids [46], etc. The final rGO products showed significantly different properties depending on their reducing potential and reaction mechanisms. As a result, the C/O ratio ranges from 30 to 2.2, and the conductivities changed from  $3.2 \times 10^{-5}$  to  $55,088 \text{ S m}^{-1}$  [41,45–47].

The need to produce rGO with programmed amounts of oxygen calls for the definition of efficient reduction protocols. Here, we compare two chemical processes, based on hydroiodic acid and sodium borohydride, and the rGO samples produced by varying the reductant concentration. The surface chemistry was analyzed using X-ray photoelectron spectroscopy and correlated to the reductant's concentration. The comparison between the two reduction chemical routes will enable the definition of optimal operation conditions and the limits of the processes.

## 2. Experimental

### 2.1. Chemicals

A water suspension of GO with concentration of 4 mg/mL was purchased from Graphenea (San Sebastian, Spain) with a monolayer content higher than 95% (measured in 0.05 wt% suspensions) and was used for the reduction process. HI (57 wt%, 99.999%),  $\text{NaBH}_4$  (98%), NaOH (97%), and ethanol (99.5%) were purchased from Sigma-Aldrich-Merck (Darmstadt, Germany) and used as received. Milli-Q water was used in the whole reduction process.

### 2.2. Reduction of Graphene Oxide with HI

rGO samples obtained using HI were prepared following the procedure in our previous report [48]. Eight samples were obtained by using 0.06 M, 0.12 M, 0.24 M, 0.47 M, 0.95 M, 1.89 M, 3.79 M, and 7.58 M HI concentrations. In a typical synthesis, 50 mL of 0.8 mg/mL GO solution was first prepared by diluting the Graphenea GO suspension and ultrasonicated for 5 min. Next, 50 mL of HI solution was added into above solution and ultrasonicated for another 5 min. The flask with above mixture was transferred into an oil bath at  $90^\circ\text{C}$  and the reduction reaction was kept at this temperature for 4h. When the reaction finished, the flask was cooled down with an ice bath. The product in the flask was collected by using a cellulose filtration paper. The rGO product was then repeatedly washed with water and ethanol and vacuum dried overnight.

### 2.3. Reduction of Graphene Oxide with $\text{NaBH}_4$

The  $\text{NaBH}_4$ -reduced rGO samples were synthesized with a previously reported procedure, although with some modifications [49]. First, 12.5 mL of GO suspension was diluted with Milli-Q water to 1.0 mg/mL under ultrasonication. Next, a  $\text{NaBH}_4$  solution was prepared by dissolving varied amounts (50 mg, 300 mg, 600 mg, 900 mg, and 1200 mg) of  $\text{NaBH}_4$  in 50 mL of NaOH solution (pH = 9). The  $\text{NaBH}_4$ —NaOH solution was slowly added into the GO solution. The mixture was then heated to  $80^\circ\text{C}$  in an oil bath and the reaction proceeded at this temperature under continuous stirring for 1h. The rGO product was collected by filtration and washed repeatedly with water and ethanol before vacuum drying overnight.

### 2.4. Characterization

X-ray photoelectron spectroscopy was utilized to study the surface chemical composition of the samples. A Kratos Axis DLD Ultra (Manchester, UK) instrument was used to carry out the spectral investigation. Thin rGO films, obtained by the two chemical routes described above, were dried under vacuum overnight for degassing and drying. For all the HI and  $\text{NaBH}_4$  concentrations, the rGO samples' conductivity was high enough to ensure the acquisition of high-quality spectra without charge compensation. For each sample, a wide spectrum was acquired at a pass energy of 150 eV to control the presence of residuals from the reduction processes. The high-resolution C 1s and O 1s core-lines were acquired using a 20 eV pass energy and an energy step of 0.05 eV. These acquisition conditions were

sufficient to study the chemical bonds and the associated concentrations. The obtained spectra were analyzed using home-made RxpsG software based on the R platform [50].

### 3. Results and Discussion

Information about the reductant concentration for each rGO sample is summarized in Table 1. rGO samples from the HI reduction and NaBH<sub>4</sub> reduction processes are denoted as S\_Hx and S\_Nx, respectively.

**Table 1.** Summary of the rGO produced using HI and NaBH<sub>4</sub>. The correspondent reductant concentrations are indicated.

| Sample Name | HI Concentration | Sample Name | NaBH <sub>4</sub> Amount |
|-------------|------------------|-------------|--------------------------|
| GO          | //               |             |                          |
| S_H1        | 0.06 M           | S_N1        | 50 mg                    |
| S_H2        | 0.12 M           | S_N2        | 300 mg                   |
| S_H3        | 0.24 M           | S_N3        | 600 mg                   |
| S_H4        | 0.47 M           | S_N4        | 900 mg                   |
| S_H5        | 0.95 M           | S_N5        | 1200 mg                  |
| S_H6        | 1.89 M           |             |                          |
| S_H7        | 3.79 M           |             |                          |
| S_H8        | 7.58 M           |             |                          |

The extent of reduction was controlled by XPS. Figure 1A shows the wide spectra obtained from the rGO samples obtained using HI as a reductant.

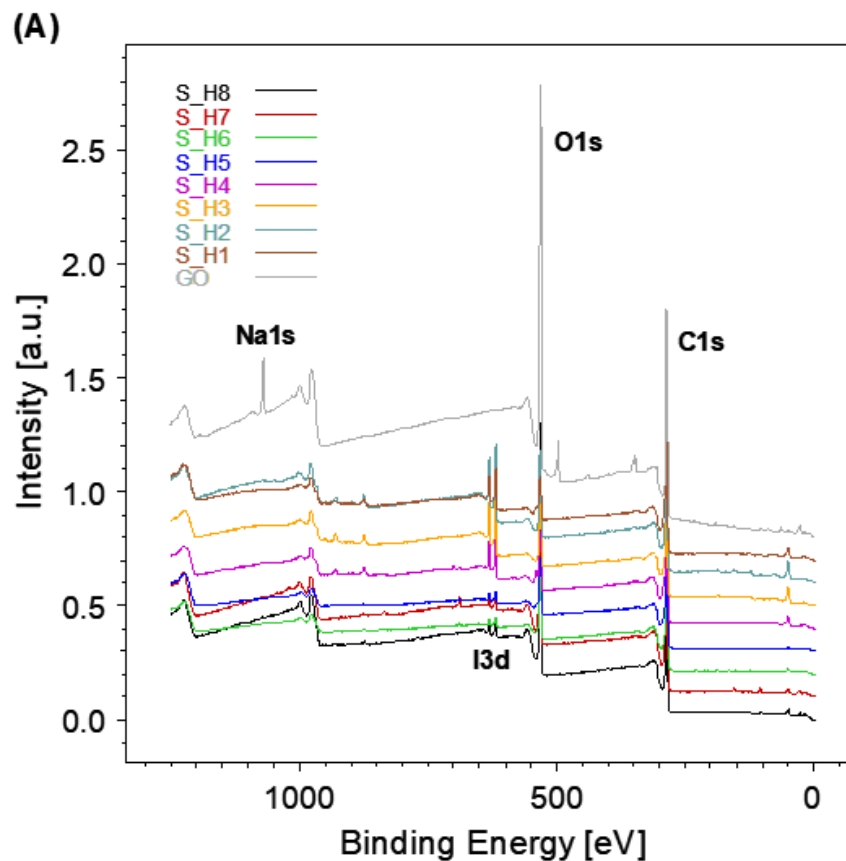


**Figure 1.** Cont.

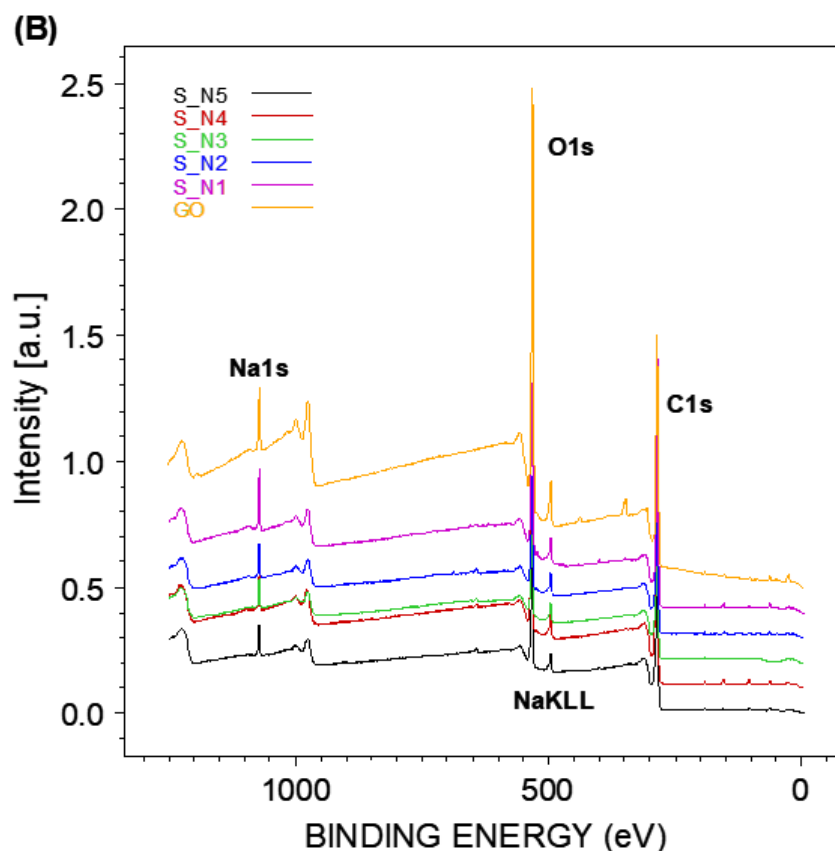


**Figure 1.** (A) Wide spectra of rGO samples synthesized using HI at increasing concentrations. The wide spectrum of GO is plotted as a reference. (B) Wide spectra of rGO samples synthesized using  $\text{NaBH}_4$  at increasing concentrations. All the spectra are normalized to the C 1s intensities to highlight O 1s variations and shifted along the Y axis to better show the spectral features. The main spectral components are indicated in both figures.

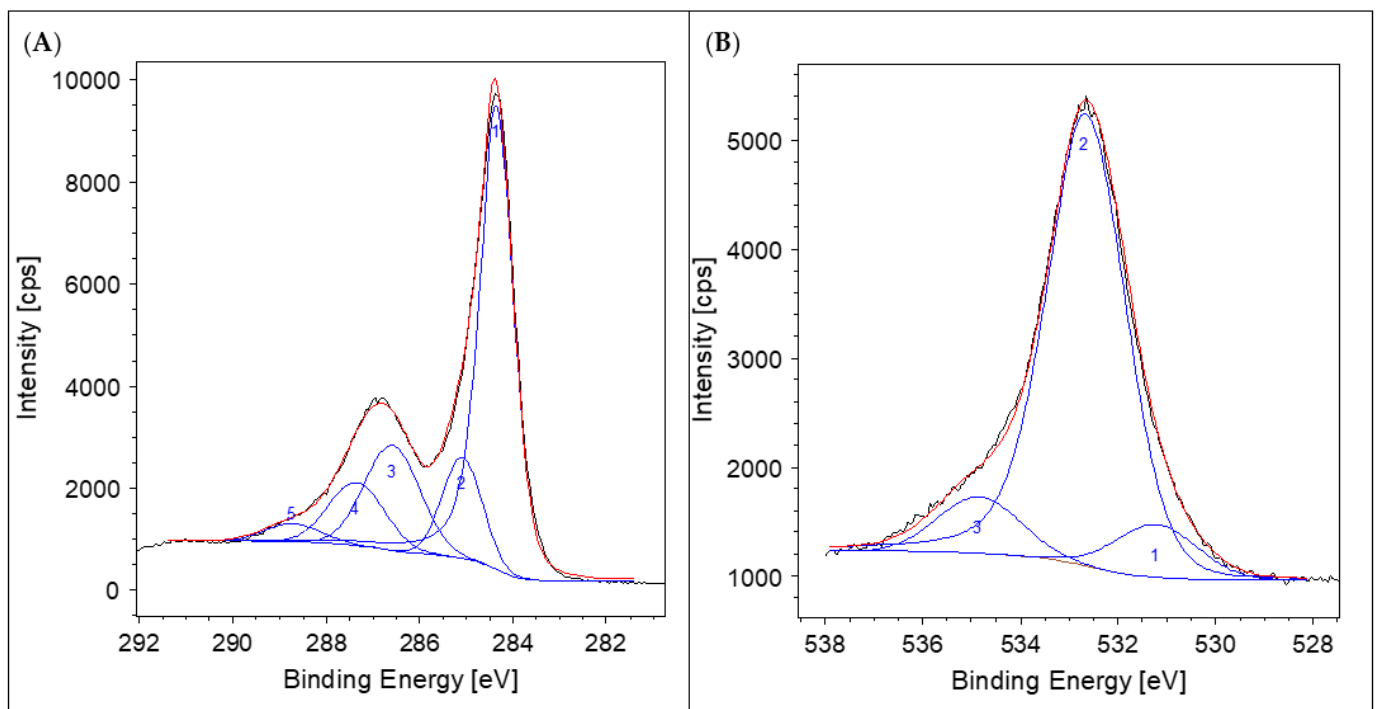
The wide spectra show that the rGO samples are composed by only carbon and oxygen, with residuals of iodine derived from the HI. In GO, iodine is absent, while the wide spectrum reveals a small Na impurity derived from the synthesis process. To compare the spectra, the intensities were normalized with respect to the C 1s. As can be seen from the spectra, by increasing the concentration of the HI in the solution, the GO undergoes a progressive reduction. This is clearly visible following the intensity of the O 1s, which is expectedly higher in the GO sample and gradually decreases with increasing HI concentration (see also Table 2). A similar behavior is found when analyzing the GO reduced using  $\text{NaBH}_4$ , as shown in Figure 1B. In addition, in this case, all the spectra are normalized with respect to the intensity of the C 1s core-line. This highlights the rapid decrease of the oxygen intensity corresponding to the initial values of the reductant concentrations. Next, there is a much slower decrease of the oxygen concentration with an increasing concentration of  $\text{NaBH}_4$  (see O concentration trend in Table 2).

In addition to carbon and oxygen, the wide spectra also display the presence of other elements derived from the chemical processing. In particular, at a high BE, a sharp peak due to Na is visible. This also introduces the Auger KLL component near the oxygen core-line. Boron 1s is hardly visible in some of the wide spectra at ~190 eV due to the very low cross section of this element. Regarding the core-line spectra, the high resolution C 1s and O 1s spectra were then fitted to follow the changes of the surface chemistry mirrored by variations of the bonding. Examples of high resolution C 1s and O 1s spectra, together with the correspondent peak fitting, are illustrated in Figure 2A,B. Figure 2A shows a main

peak assigned to the  $sp^2$  graphitic phase of the S\_H2 sample. The fitting component is characterized by a certain asymmetry, mirroring the semimetallic property associated with this phase. The degree of asymmetry may be associated with the reconstruction of the C–C aromatic bonds typical of the graphene structure. This causes the occurrence of energy loss processes described by the pronounced intensity of the C 1s tail at high binding energy. The semimetallic character of the graphitic C 1s component is the reason for selecting a Shirley base-line for the background subtraction. A Gaussian lineshape was used for the other fitting components needed to describe the other chemical bonds. The first component at  $\sim 285$  eV is derived from hydrocarbon contaminations. Component 3 at 286.2 eV is assigned to the hydroxyl and epoxy-like bonds, while the component at  $\sim 287.5$  eV is assigned to the carbonyl bond and carbon atoms bonded to two oxygen atoms in a –O–C–O– bond [51,52].

**Table 2.** Oxygen and carbon–oxygen concentrations.

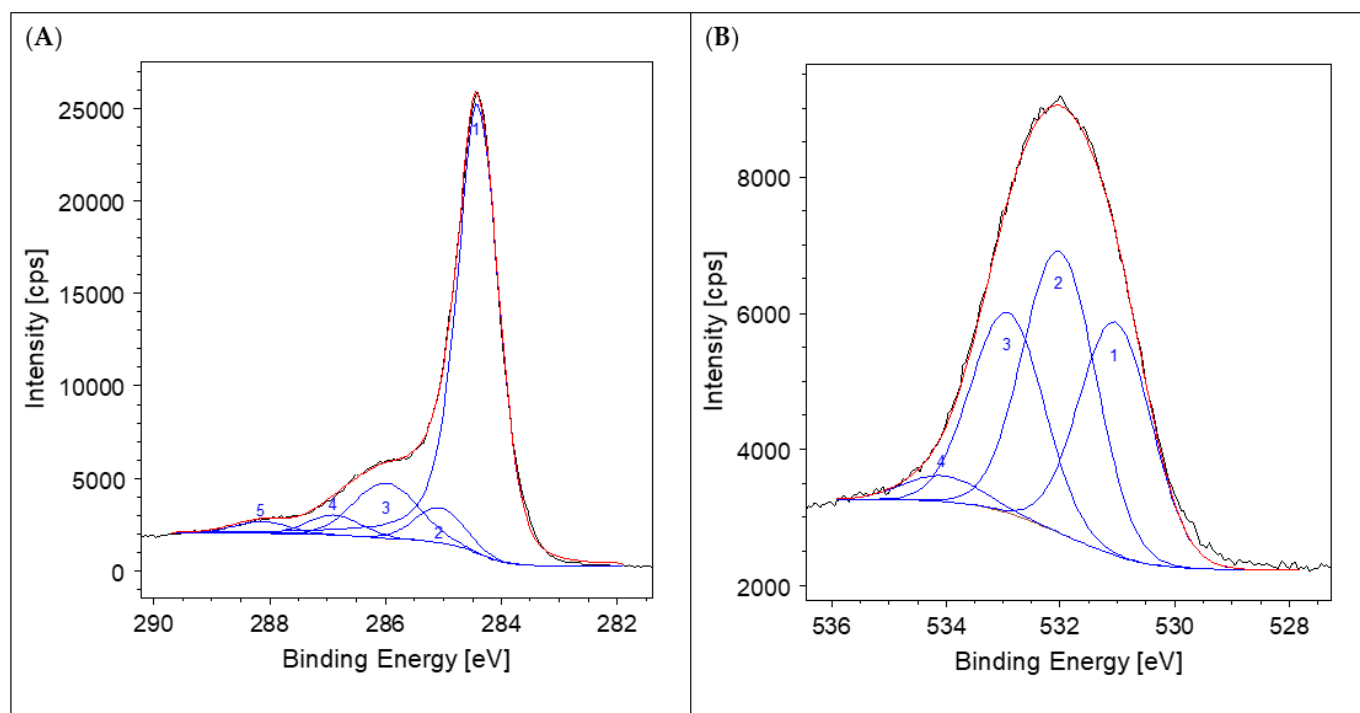
| Sample | O conc. (%) | CO <sub>x</sub> conc. (%) | Sample | O conc. (%) | CO <sub>x</sub> conc. (%) |
|--------|-------------|---------------------------|--------|-------------|---------------------------|
| GO     | 32.34       | 30.02                     | S_N1   | 30.02       | 32.34                     |
| S_H1   | 21.86       | 22.24                     | S_N2   | 13.59       | 13.07                     |
| S_H2   | 16.94       | 16.96                     | S_N3   | 9.78        | 9.97                      |
| S_H3   | 10.50       | 10.98                     | S_N4   | 8.91        | 8.91                      |
| S_H4   | 10.29       | 10.21                     | S_N5   | 8.62        | 8.63                      |
| S_H5   | 9.09        | 9.01                      |        |             |                           |
| S_H6   | 8.06        | 8.52                      |        |             |                           |
| S_H7   | 7.72        | 7.76                      |        |             |                           |
| S_H8   | 5.32        | 5.77                      |        |             |                           |



**Figure 2.** (A) C 1s and (B) O 1s core-lines of the S\_H2 sample reported together with their peak fitting.

Finally, the carboxyl bond is found at a higher BE. Similar peak fitting was performed on the C 1s from the other HI-reduced rGO samples. In the case of oxygen, the core-

lines were fitted using three Gaussian components, as reported in Figure 2B. The first two components are assigned to carbon–oxygen bonds and, specifically, to C=O bonds at lower BE and C–O single bonds at the higher BE. The remaining third fitting component at ~534 eV (or higher) is derived from oxygen in H<sub>2</sub>O molecules adsorbed on the surfaces of rGO-HI samples [51,52]. A similar interpretation also holds for the C 1s and O 1s core-lines from the rGO-NaBH<sub>4</sub> samples. Figure 3A,B reports an example of the peak fitting of the two core-lines. As seen in Figure 1B, residuals of Na are present in all the S<sub>N</sub> samples. One final note regarding the complete overlap of the Auger KL<sub>1</sub>L<sub>23</sub> component falling at 532 eV: in all the peak fittings of the oxygen core-lines, the contribution of this Auger component is negligible and, for this reason, it was ignored. As in the previous case, a Shirley baseline was utilized for the background subtraction of the high-resolution C 1s spectrum. In addition, the main peak corresponding to the sp<sup>2</sup> phase is described by an asymmetric lineshape to account for the energy losses according to the notes above. The remaining components are Gaussian and are assigned to the chemical bonds previously described. Component 2 at ~285.0 eV is assigned to hydrocarbon contamination. At increasing BE, hydroxyl and epoxy, carbonyl, O–C–O bonds, and carboxyl groups can be found, respectively. There are differences in the peak fitting of the oxygen core-line. The components at lower BE are assigned to contributions derived from NaOH and NaHBO<sub>3</sub>. The two components at ~532 and ~532.7 eV are assigned to carbon–oxygen bonds, while the component at the higher BE accounts for the oxygen derived from adsorbed H<sub>2</sub>O molecules.



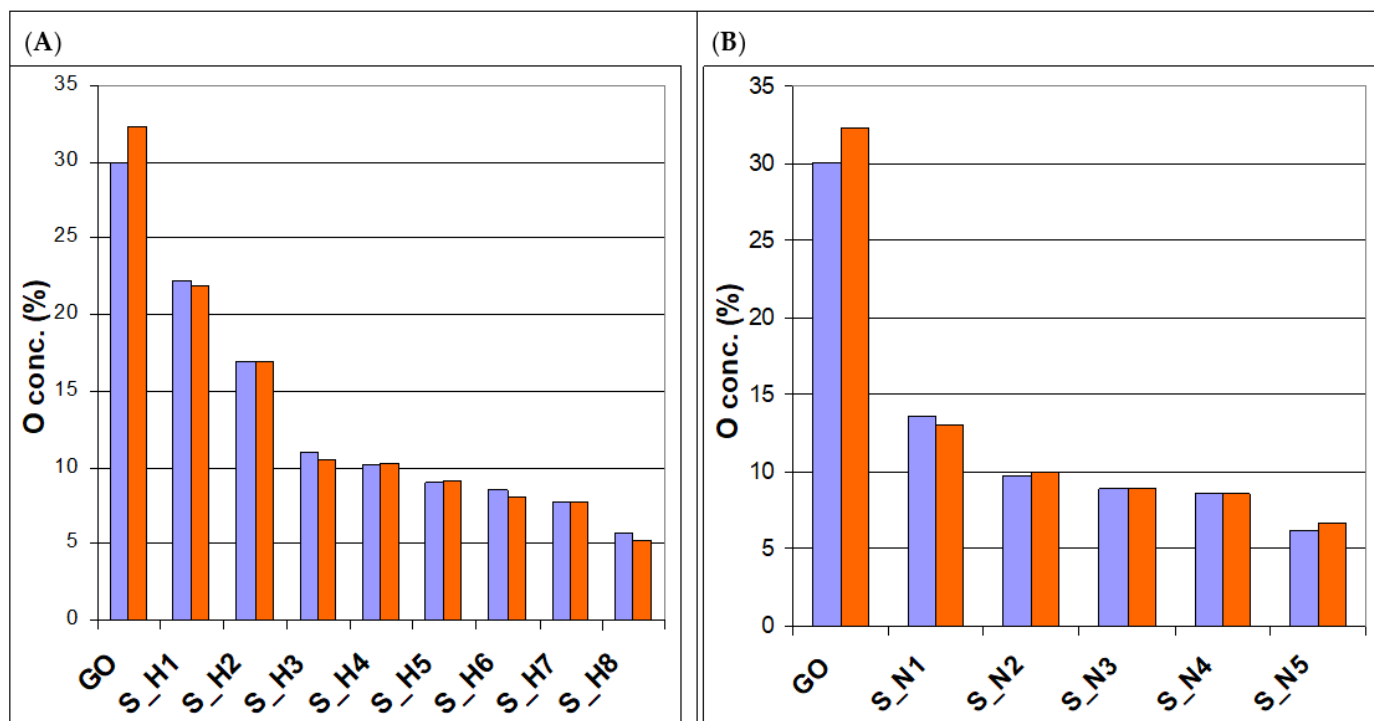
**Figure 3.** (A) C 1s and (B) O 1s core-lines of the S<sub>N</sub>3 sample reported together with their peak fitting.

Figure 4A,B shows the trend of oxygen concentrations in S<sub>H</sub> and S<sub>N</sub> samples.

Increasing the amounts of HI and NaBH<sub>4</sub> reductants in the GO water suspension results in a reduction of the concentration of oxygen in both cases. Interestingly, an excellent agreement between the oxygen concentration and the abundance of the oxidized carbon components is obtained. The latter was estimated considering the stoichiometry of the carbon–oxygen bond described by the various fit components.

As illustrated in Figure 4, for both HI and NaBH<sub>4</sub>, a higher effect is obtained at the beginning, where a lower reductant concentration corresponds to a higher decrease of oxygen. Consequently, the abundances of carbon atoms involved in bonds with oxygen

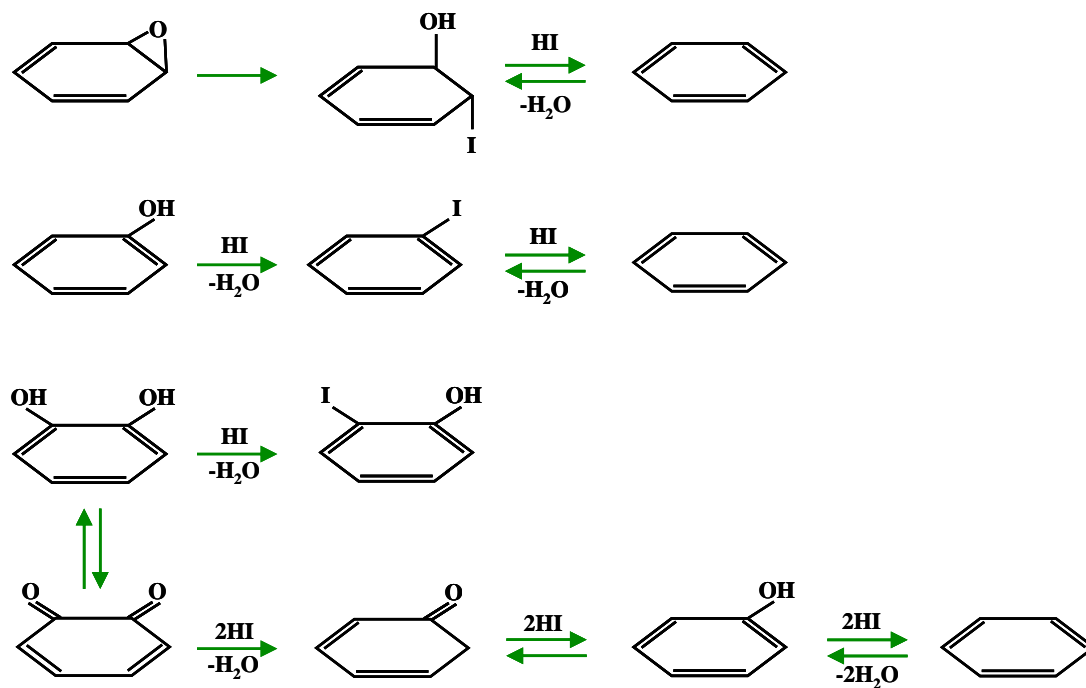
show the same behavior, having a tendency to display a flattening of the trend. Table 2 summarizes the values of the oxygen and C–O<sub>x</sub> concentrations for the various reductant concentrations.



**Figure 4.** Trend of the total oxygen concentrations (blue) and of the concentration of oxygen derived from the C1s fit and carbon oxidized fit components of carbon (red) in rGO reduced using HI (A) or NaBH<sub>4</sub> (B).

HI, as well as other hydrohalic acids such as HBr and HCl, is used in the electrophilic addition and nucleophilic substitution chemical reactions. Considering the nucleophilic nature of halides, I<sup>−</sup> possesses a higher nucleophilicity with respect to Cl<sup>−</sup> and Br<sup>−</sup>. In addition, HI is very efficient in attacking epoxide C–O bonds [47]. This renders HI the reductant of choice to remove oxygen from GO hydroxyl and epoxy bonds, which constitute the main portion of the carbon–oxygen bonds. In Figure 5A, a representative scheme of the possible chemical reactions that can occur between HI and GO is presented. In agreement with these reaction models, the cleavage of ether and iodination, iodination of alcohols, reduction of aromatic iodides, and partial reduction of the carbonyl groups may occur [44]. This could also explain why the reaction of GO with an increasing concentration of HI leads to a progressive decrease of the reduction efficiency. When hydroxyl and epoxy groups are largely removed, the other kind of bonds, such as carboxyl, lactone, –O–C–O–, and carbonyl groups, are likely still present on the rGO surface, as can be seen in the high-resolution C 1s spectra. As a matter of fact, in our GO sample, the hydroxyl and epoxy groups amount to ~24% of the total oxygen concentration, which is reported as 30% in Table 2. The remaining part of the carbon–oxygen bonds, which is around 6%, corresponds to the percentage of the oxygen left on the sample surface after the reduction with higher HI concentrations (see the CO<sub>x</sub> concentration in Table 2), which is in good agreement with the residual oxygen abundance found in the S\_H8 sample.

(A)



(B)

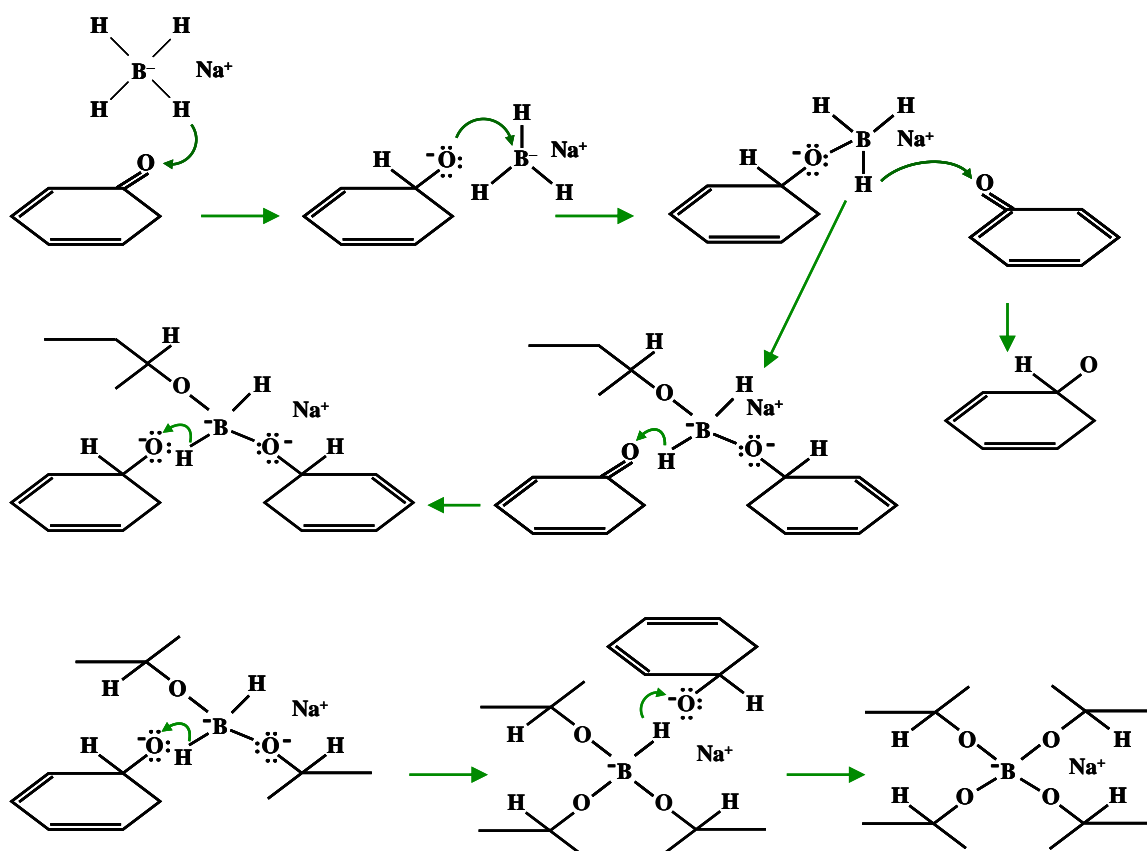
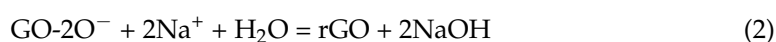
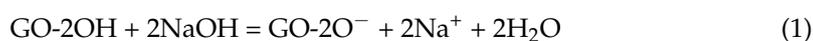


**Figure 5.** (A) Model of the chemical reaction occurring between oxygen-containing aromatic groups and HI; (B) progression of carbonyl group reduction until the complete depletion of B-H bonds and boron oxidation.

Regarding the use of  $\text{NaBH}_4$ , this is a compound containing a  $\text{BH}_4^-$  anion with a tetrahedral structure. In aqueous solution, this anion reacts easily with electrophile species, such as carbonyl groups, as illustrated in Figure 5B. The borohydride anion induces a hydride transfer reaction, resulting in an oxyanion and an electron-deficient  $\text{BH}_3$  molecule. The oxyanion can then react with  $\text{BH}_3$ , restoring the borohydride. This reaction proceeds until B–H bonds have been depleted. In reality, this ideal reaction scheme does not occur in common reduction processes, where the reduction efficiency is related to the kind of original compound.  $\text{NaBH}_4$  is able to react with aldehyde and ketone carbonyl groups, while carbonyl compounds, such as esters or amides, are not reducible. However, a simulation report showed that, in a  $\text{NaOH}$  solution, the  $\text{OH}^-$  anion can interact with a hydroxyl group in GO to generate negatively charged GO. Due to this electron transfer, it is easy for the epoxy ring to be opened with a small energy barrier. These oxygen atoms on negatively charged GO can be removed with the assistance of  $\text{Na}^+$  and a water molecule. In this process,  $\text{NaOH}$  can be considered as a catalyst [53]. The reduction reactions are listed below:



As apparent from Figure 4B, the trend of the oxygen concentration is similar to that obtained using HI. Additionally, the lower value of oxygen corresponding to the higher value of  $\text{NaBH}_4$  concentration is comparable to that from the HI reduction process. We can then hypothesize that, in this case,  $\text{NaBH}_4$  primarily removes hydroxyl and epoxy groups. This hypothesis is confirmed by the results reported previously [54], where the authors studied the trend of carbon–oxygen single and double bonds as a function of the reduction reaction time. The authors found that the concentration of carbonyl bonds remains more or less constant with time, while C–O single bonds undergo a decrease when increasing the reaction time. These findings are also in agreement with the work of other authors, where  $\text{NaBH}_4$  preserved carboxyl groups useful for the further functionalization of the rGO sheets [55]. These results are partially in agreement with other results showing that  $\text{NaBH}_4$  transforms the carbonyl in hydroxyl groups, which is subsequently removed along with epoxy bonds [43]. The decreasing efficiency of the reductant already found for HI at increasing concentrations is also found in the case of  $\text{NaBH}_4$ . In addition, in this case, the reduction of the oxygen abundance when increasing the concentration of  $\text{NaBH}_4$  deviates from a linear trend and shows saturation. This is in agreement with other studies reporting a similar trend of the residual oxygen in rGO vs  $\text{NaBH}_4$  concentration [43] or vs increasing reduction time processing [54]. Interestingly, the residual oxygen concentration left on the S\_N5 sample is much lower than that obtained in [43,54] after a reaction time of 24 h.

#### 4. Conclusions

The increasing demand of producing high-quality reduced graphene oxide possessing high conductivity and low defect density has motivated this study, which was aimed at comparing the efficiency of hydroiodic acid and sodium borohydride. These chemical compounds are known to be active towards oxidized species, but their reactivity varies upon the nature of the bond formed by oxygen. XPS was then used to shed light on the reaction mechanisms at the basis of the GO reduction. Characterization analyses were performed at increasing reductant concentration. Results show that, for both HI and  $\text{NaBH}_4$ , the initial reduction process proceeds efficiently. However, when the residual oxygen concentration lowers, the reaction with oxygen atoms, and their successive removal, becomes more complex. As such, results show that, at the higher HI and  $\text{NaBH}_4$  concentration, the residual oxygen concentration is minimal and lower with respect to that found by other studies where these reductant agents were utilized. As a matter of fact, results show that the final oxygen concentrations are 5.3% and 8.6%, making HI more efficient than  $\text{NaBH}_4$ – $\text{NaOH}$ . The improved sheet degree of GO reduction may open up more practical uses of this

material in all of the applicative sectors where electrical properties of the material play an important role.

**Author Contributions:** Conceptualization, G.S.; Data curation, G.S. and W.L.; Formal analysis, G.S. and W.L.; Writing—original draft, G.S.; Writing—review & editing, W.L. All authors have read and agreed to the published version of the manuscript.

**Funding:** This research received no external funding.

**Data Availability Statement:** The data presented in this study are available from the corresponding author upon request.

**Conflicts of Interest:** The authors declare no conflict of interest.

## References

1. Georgakilas, V.; Perman, J.A.; Tucek, J.; Zboril, R. Broad Family of Carbon Nanoallotropes: Classification, Chemistry, and Applications of Fullerenes, Carbon Dots, Nanotubes, Graphene, Nanodiamonds, and Combined Superstructures. *Chem. Rev.* **2015**, *115*, 4744–4822. [[CrossRef](#)] [[PubMed](#)]
2. Allen, M.J.; Tung, V.C.; Kaner, R.B. Honeycomb carbon: A review of graphene. *Chem. Comm.* **2010**, *110*, 132–145. [[CrossRef](#)] [[PubMed](#)]
3. Kong, W.; Kum, H.; Bae, S.-H.; Shim, J.; Kim, H.; Kong, L.; Meng, K.; Wang, K.; Kim, C.; Kim, J. Path towards graphene commercialization from lab to market. *Nat. Nanotechnol.* **2019**, *14*, 927–938. [[CrossRef](#)] [[PubMed](#)]
4. Chen, D.; Feng, H.; Li, J. Graphene Oxide: Preparation, Functionalization, and Electrochemical Applications. *Chem. Rev.* **2012**, *112*, 6027–6053. [[CrossRef](#)]
5. Wang, Y.; Li, S.; Yang, H.; Luo, J. Progress in the functional modification of graphene/graphene oxide: A review. *RSC Adv.* **2020**, *10*, 15328.
6. Xiong, Y.; Xie, Y.; Zhang, F.; Ou, E.; Jiang, Z.; Ke, L.; Hu, D.; Xu, W. Reduced graphene oxide/hydroxylated styrene-butadiene-styrene tri-block copolymer electroconductive nanocomposites: Preparation and properties. *Mater. Sci. Eng. B* **2012**, *177*, 1157–1163. [[CrossRef](#)]
7. Joshi, D.J.; Koduru, J.R.; Malek, N.I.; Hussain, C.M.; Kailasa, S.K. Surface modifications and analytical applications of graphene oxide: A review. *Trends Anal. Chem.* **2021**, *144*, 116448. [[CrossRef](#)]
8. Shareena, T.P.D.; McShan, D.; Dasmahapatra, A.K.; Tchounwou, P.B. A Review on Graphene-Based Nanomaterials in Biomedical Applications and Risks in Environment and Health. *Nano-Micro Lett.* **2018**, *10*, 53. [[CrossRef](#)]
9. Liu, Y.; Dong, X.; Chen, P. Biological and chemical sensors based on graphene materials. *Chem. Soc. Rev.* **2012**, *41*, 2283–2307. [[CrossRef](#)]
10. Ahmad, H.; Fan, M.; Hui, D. Graphene oxide incorporated functional materials: A review. *Compos. B* **2018**, *145*, 270–280. [[CrossRef](#)]
11. Wang, Z.; Nelson, J.K.; Hillborg, H.; Zhao, S.; Schadler, L.S. Graphene Oxide Filled Nanocomposite with Novel Electrical and Dielectric Properties. *Adv. Mater.* **2012**, *24*, 3134–3137. [[CrossRef](#)] [[PubMed](#)]
12. Türkaslan, S.S.; Ugur, S.S.; Türkaslan, B.E.; Fantuzzi, N. Evaluating the X-ray-Shielding Performance of Graphene-Oxide-Coated Nanocomposite Fabric. *Materials* **2022**, *15*, 1441. [[CrossRef](#)] [[PubMed](#)]
13. Chauhan, D.S.; Quraishi, M.A.; Ansari, K.R.; Saleh, T.A. Graphene and graphene oxide as new class of materials for corrosion control and protection: Present status and future scenario. *Progr. Org. Coat.* **2020**, *147*, 105741. [[CrossRef](#)]
14. Obayomi, K.S.; Lau, S.Y.; Danquah, M.; Chiong, T.; Takeo, M. Advances in graphene oxide based nanobiocatalytic technology for wastewater treatment. *Environ. Nanotechnol. Monit. Manag.* **2022**, *17*, 100647. [[CrossRef](#)]
15. Siwinska-Stefanska, K.; Fluder, M.; Tylus, W.; Jesionowski, T. Investigation of amino-grafted TiO<sub>2</sub>/reduced graphene oxide hybrids as a novel photocatalyst used for decomposition of selected organic dyes. *J. Environ. Manag.* **2018**, *212*, 395–404. [[CrossRef](#)]
16. Perreault, F.; de Faria, A.F.; Elimelech, M. Environmental applications of graphene-based nanomaterials. *Chem. Soc. Rev.* **2015**, *44*, 5861–5896. [[CrossRef](#)] [[PubMed](#)]
17. Tian, Y.; Yu, Z.; Cao, L.; Zhang, L.X.; Sun, C.; Wang, D.W. Graphene oxide: An emerging electromaterial for energy storage and conversion. *J. Energy Chem.* **2021**, *55*, 323–344. [[CrossRef](#)]
18. Chen, K.; Song, S.; Liu, F.; Xue, D. Structural design of graphene for use in electrochemical energy storage devices. *Chem. Soc. Rev.* **2015**, *44*, 6230–6257. [[CrossRef](#)]
19. Guo, S.; Dong, S. Graphene nanosheet: Synthesis, molecular engineering, thin film, hybrids, and energy and analytical applications. *Chem. Soc. Rev.* **2011**, *40*, 2644–2672. [[CrossRef](#)]
20. Kamedulski, P.; Truszkowski, S.; Lukaszewicz, J.P. Highly Effective Methods of Obtaining N-Doped Graphene by Gamma Irradiation. *Materials* **2020**, *13*, 4975. [[CrossRef](#)]
21. Mankge, N.S.; Madito, M.J.; Hlongwa, N.W.; Kuvarega, A.T. Review of electrochemical production of doped graphene for energy storage applications. *J. Energy Storage* **2022**, *46*, 103527. [[CrossRef](#)]

22. Velasco-Soto, M.A.; Perez-Garcia, S.A.; Alvarez-Quintana, J.; Cao, Y.; Nyborg, L.; Licea-jimenez, L. Selective band gap manipulation of graphene oxide by its reduction with mild reagents. *Carbon* **2015**, *93*, 967–973. [[CrossRef](#)]
23. Shen, Y.; Yang, S.; Zhou, P.; Sun, Q.; Wang, P.; Wan, L.; Li, J.; Chen, L.; Wang, X.; Ding, S.; et al. Evolution of the band-gap and optical properties of graphene oxide with controllable reduction level. *Carbon* **2013**, *62*, 157–164. [[CrossRef](#)]
24. Hasan, M.T.; Senger, B.J.; Ryan, C.; Culp, M.; Gonzalez-Rodriguez, R.; Coffey, J.L.; Naumov, A.V. Optical Band Gap Alteration of Graphene Oxide via Ozone Treatment. *Sci. Rep.* **2017**, *7*, 6411. [[CrossRef](#)]
25. Weiss, N.O.; Zhou, H.; Liao, L.; Liu, Y.; Jiang, S.; Huang, Y.; Duan, X. Graphene: An emerging electronic material. *Adv. Mater.* **2012**, *24*, 5782–5825. [[CrossRef](#)]
26. Gupta, S.; Joshi, P.; Narayan, J. Electron mobility modulation in graphene oxide by controlling carbon melt lifetime. *Carbon* **2020**, *170*, 327–3337. [[CrossRef](#)]
27. Lee, C.; Wei, X.; Kysar, J.W.; Hone, J. Measurement of the elastic properties and intrinsic strength of monolayer graphene. *Science* **2008**, *321*, 385–388. [[CrossRef](#)]
28. Liu, L.; Zhang, J.; Zhao, J.; Liu, F. Mechanical properties of graphene oxides. *Nanoscale* **2012**, *4*, 5910–5916. [[CrossRef](#)] [[PubMed](#)]
29. Nair, R.R.; Blake, P.; Grigorenko, A.N.; Novosdelov, K.S.; Booth, T.J.; Stauber, T.; Peres, N.M.R.; Geim, A.K. Fine Structure Constant Defines Visual Transparency of Graphene. *Science* **2008**, *320*, 1308. [[CrossRef](#)]
30. Su, R.; Lin, S.F.; Chen, D.Q.; Chen, G.H. Study on the Absorption Coefficient of Reduced Graphene Oxide Dispersion. *J. Phys. Chem. C* **2014**, *118*, 12520–12525. [[CrossRef](#)]
31. Jin, Y.; Zheng, Y.; Podkolzin, S.G.; Lee, W. Band gap of reduced graphene oxide tuned by controlling functional groups. *J. Mater. Chem. C* **2020**, *8*, 4885–4894. [[CrossRef](#)]
32. Sehrawat, A.P.; Islam, S.S.; Mishra, P.; Ahmad, S. Reduced graphene oxide (rGO) based wideband optical sensor and the role of Temperature, Defect States and Quantum Efficiency. *Sci. Rep.* **2018**, *8*, 3537.
33. Wang, Y.; Wang, L.; Wang, H.Y.; Chen, Q.D.; Sun, H.B. Ultrafast Spectroscopic Study of Insulator-Semiconductor-Semimetal Transitions in Graphene Oxide and Its Reduced Derivatives. *J. Phys. Chem. C* **2019**, *123*, 22550–22555. [[CrossRef](#)]
34. Bhaumik, A.; Haque, A.; Taufique, M.; Karnati, P.; Patel, R.; Nath, M.; Ghosh, K. Reduced Graphene Oxide Thin Films with Very Large Charge Carrier Mobility Using Pulsed Laser Deposition. *J. Mater. Sci. Eng.* **2017**, *6*, 4. [[CrossRef](#)]
35. Wang, Y.; Chen, Y.; Lacey, S.D.; Xu, L.; Xie, H.; Li, T.; Danner, V.A.; Hu, L. Reduced graphene oxide film with record-high conductivity and mobility. *Mater. Today* **2018**, *21*, 186–192. [[CrossRef](#)]
36. Mohan, V.B.; Brown, R.; Jayaraman, K.; Bhattacharyya, D. Characterisation of reduced graphene oxide: Effects of reduction variables on electrical conductivity. *Mater. Sci. Eng. B* **2015**, *193*, 49–60. [[CrossRef](#)]
37. Tarcan, R.; Todor-Boer, O.; Petrovai, I.; Leordean, C.; Astilean, S.; Botiz, I. Reduced graphene oxide today. *J. Mater. Chem. C* **2020**, *8*, 1198–1224. [[CrossRef](#)]
38. Smith, A.T.; LaChance, A.M.; Zeng, S.; Liu, B.; Sun, L. Synthesis, properties, and applications of graphene oxide/reduced graphene oxide and their nanocomposites. *Nano Mater. Sci.* **2019**, *1*, 31–47. [[CrossRef](#)]
39. Agarwal, V.; Zetterlund, P.B. Strategies for reduction of graphene oxide—A comprehensive review. *Chem. Eng. J.* **2021**, *405*, 127018. [[CrossRef](#)]
40. Park, S.; An, J.; Potts, J.R.; Velamakanni, A.; Murali, S.; Ruoff, R.S. Hydrazine-reduction of graphite- and graphene oxide. *Carbon* **2011**, *49*, 3019–3023. [[CrossRef](#)]
41. Zhang, J.; Yang, H.; Shen, G.; Cheng, P.; Zhang, J.; Guo, S. Reduction of graphene oxide via ascorbic acid. *Chem. Commun.* **2010**, *46*, 1112–1114. [[CrossRef](#)] [[PubMed](#)]
42. Zhang, C.; Lv, W.; Zhang, W.; Zheng, X.; Wu, M.-B.; Wei, W.; Tao, Y.; Li, Z.; Yang, Q. Reduction of Graphene Oxide by Hydrogen Sulfide: A Promising Strategy for Pollutant Control and as an Electrode for Li-S Batteries. *Adv. Energy Mater.* **2014**, *4*, 1301565. [[CrossRef](#)]
43. Shin, H.-J.; Kim, K.K.; Benayad, A.; Yoon, S.-M.; Park, H.K.; Jung, I.-S.; Jin, M.H.; Jeong, H.-K.; Kim, J.M.; Choi, J.-Y.; et al. Efficient Reduction of Graphite Oxide by Sodium Borohydride and Its Effect on Electrical Conductance. *Adv. Funct. Mater.* **2009**, *19*, 1987–1992. [[CrossRef](#)]
44. Moon, I.K.; Lee, J.; Ruoff, R.S.; Lee, H. Reduced graphene oxide by chemical graphitization. *Nat. Comm.* **2010**, *1*, 73. [[CrossRef](#)] [[PubMed](#)]
45. Liu, C.; Hao, F.; Zhao, Q.; Luo, S.; Lin, H. Low temperature reduction of free-standing graphene oxide papers with metal iodides for ultrahigh bulk conductivity. *Sci. Rep.* **2014**, *4*, 3965. [[CrossRef](#)] [[PubMed](#)]
46. Chen, D.; Li, L.; Guo, L. An environment-friendly preparation of reduced graphene oxide nanosheets via amino acid. *Nanotechnology* **2011**, *22*, 325601. [[CrossRef](#)]
47. Chua, C.K.; Pumera, M. Chemical reduction of graphene oxide: A synthetic chemistry viewpoint. *Chem. Soc. Rev.* **2014**, *43*, 291–312. [[CrossRef](#)]
48. Liu, W.; Speranza, G. Tuning the Oxygen Content of Reduced Graphene Oxide and Effects on Its Properties. *ACS Omega* **2021**, *6*, 6195–6205. [[CrossRef](#)]
49. Tan, S.M.; Ambrosi, A.; Chua, C.K.; Pumera, M. Electron transfer properties of chemically reduced graphene materials with different oxygen contents. *J. Mater. Chem. A* **2014**, *2*, 10668–10675. [[CrossRef](#)]
50. Speranza, G.; Canteri, R. XpysG a new open project for Photoelectron and Electron Spectroscopy data processing. *SoftwareX* **2019**, *10*, 100282. [[CrossRef](#)]

51. Moulder, J.F.; Stickle, W.F.; Sobol, P.E.; Bomben, K.D. *Handbook of X-ray Photoelectron Spectroscopy: A Reference Book of Standard Spectra for Identification and Interpretation of Xps Data*; EdenPraire, Physical Electronics: Minnesota, MN, USA, 1995.
52. Beamson, G.; Briggs, D. *High Resolution XPS of Organic Polymers: The Scienta ESCA300 Database*; Surface Spectra: Chichester, UK, 1992.
53. Chen, C.; Kong, W.; Duana, H.-M.; Zhang, J. Theoretical simulation of reduction mechanism of graphene oxide in sodium hydroxide solution. *Phys. Chem. Chem. Phys.* **2014**, *16*, 12858–12864. [[CrossRef](#)] [[PubMed](#)]
54. Guex, L.G.; Sacchi, B.; Peuvot, K.F.; Andersson, R.L.; Pourrahimi, A.M.; Strom, V.; Farris, S.; Olsson, R.T. Experimental review: Chemical reduction of graphene oxide (GO) to reduced graphene oxide (rGO) by aqueous chemistry. *Nanoscale* **2017**, *9*, 9562. [[CrossRef](#)] [[PubMed](#)]
55. Tien, H.W.; Huang, Y.L.; Yang, S.Y.; Hsiao, S.T.; Liao, W.H.; Li, H.M.; Wang, Y.S.; Wang, J.Y.; Ma, C.C.M. Preparation of transparent, conductive films by graphene nanosheet deposition on hydrophilic or hydrophobic surfaces through control of the pH value. *J. Mater. Chem.* **2012**, *22*, 2545–2552. [[CrossRef](#)]